Thermocapillary Motion of a Liquid Drop on a Horizontal Solid Surface

Vikram Pratap,† Nadjoua Moumen,‡ and R. Shankar Subramanian*

Department of Chemical Engineering and Center for Advanced Materials Processing, Clarkson University, Potsdam, New York 13699-5705

Received November 26, 2007. In Final Form: February 11, 2008

The motion of drops of decane on horizontal poly(dimethylsiloxane) (PDMS)-coated glass surfaces resulting from a temperature gradient on the surface is studied experimentally, and a theoretical description of the thermocapillary motion of spherical-cap drops on a horizontal solid surface obtained using the lubrication approximation also is presented. The drop size and the applied temperature gradient are varied in the experiments, and the measured velocities of the drops are compared with predictions from the model. The scalings of the velocity with drop size and with the applied temperature gradient are predicted correctly by the theoretical model, even though the actual velocities are smaller than those predicted. The influence of contact angle hysteresis, which leads to a critical drop size below which drops do not move, is found to be minimal. Unlike in previous studies (Chen, J. Z.; Troian, S. M.; Darhuber, A. A.; Wagner, S. *J. Appl. Phys.* **2005**, *97*, 014906; Brzoska, J. B.; Brochard-Wyart, F.; Rondelez, F. *Langmuir* **1993**, *9*, 2220), this small critical drop size appears to be independent of the applied temperature gradient. Results also are presented on the deformation of the contact lines of the moving drops in the form of an aspect ratio, and correlated with the temperature difference across the footprints of the drops and the capillary number.

1. Introduction

The term "thermocapillarity" refers to phenomena that arise as a consequence of the variation of interfacial tension at a fluid−fluid interface caused by temperature differences. Thermocapillarity can be employed as a mechanism for driving the motion of bubbles and drops immersed in a second phase. Typically, the interfacial tension decreases with increasing temperature, and this leads to the movement of bubbles or drops suspended in a second phase toward warmer regions; this subject has been studied in depth, particularly because of the impetus provided by research in orbital spacecraft as noted in Subramanian and Balasubramaniam.[1] In the present work, we focus attention on a different use of thermocapillarity, namely the use of temperature differences to drive the motion of liquid drops on a horizontal solid surface. This mechanism can be helpful in a variety of practical microfluidics applications as noted in earlier work.[2−4]

As opposed to a liquid drop fully immersed in a liquid, which moves toward warm fluid, a liquid drop placed on a horizontal solid surface moves toward cooler regions on the solid surface. This can be explained as follows. When a drop is placed on a solid surface upon which a temperature gradient has been imposed, a corresponding temperature variation arises at the liquid−gas interface. The variation of surface tension from lower values on the warm side to higher values on the cool side of the interface generates a flow in the drop, which exerts a hydrodynamic force on the solid surface that points in the direction of the applied temperature gradient. The solid surface, which is held immobile, exerts an equal and opposite reaction on the drop that propels it in the opposite direction, namely toward cooler regions. Under suitable conditions, it is possible to achieve quasisteady motion wherein the net hydrodynamic force on the drop is zero.

The idea of using a temperature difference as a driving force for moving drops appears to have been recognized first by Bouasse[5] who heated the lower end of a metal wire, tilted slightly upward, to move drops upward against the force of gravity from the heated spot toward the cold regions on the wire. A detailed study of this type of drop motion on glass fibers was undertaken by Yarin et al.[6] who locally heated a horizontally oriented glass fiber on which drops of a variety of liquids had been deposited, and observed the movement of the drops away from the source of heat. Yarin et al. also observed similar movement of drops on a locally heated copper wire. The authors presented an approximate theoretical description of the motion, along with their experimental results.

Of more direct relevance to the present work are two systematic experimental studies: one by Brzoska et al.[7] and the other by Chen et al.[4] Both groups of investigators conducted experiments on the motion of liquid drops positioned on a horizontal silanized silicon surface on which a temperature gradient was established. Brzoska et al. used poly(dimethylsiloxane) (PDMS) oils of varying viscosity for the drop material, while a major portion of the data presented and fitted with a theoretical prediction in Chen et al. was obtained on squalane drops; Chen et al. also report data obtained using several other liquids, in addition. Brzoska et al. were interested in matching the surface tension of the liquid−air interface to the critical surface tension of the silanized surfaces so as to obtain contact angles close to zero. They used relatively large drops, in the range 1−10 mm in equilibrium footprint radius, and temperature gradients ranging from 0.35 to 1.0 K/mm in their work. The drops were initially allowed to reach equilibrium on an isothermal surface and then subjected to the temperature

* To whom correspondence should be addressed. E-mail: subramanian@clarkson.edu.

† Present address: General Electric, John F. Welch Technology Center, Plot 122 EPIP Phase 2, Whitefield Road, Bangalore 560 066, India.

‡ Present address: RA1-278, 2501 NW 229th Avenue, Intel Corporation, Hillsboro, Oregon 97124.

(1) Subramanian, R. S.; Balasubramaniam, R. *The Motion of Bubbles and Drops in Reduced Gravity*; Cambridge University Press: Cambridge, 2001.

(2) Darhuber, A. A.; Valentino, J. P.; Davis, J. M.; Troian, S. M.; Wagner, S. *Appl. Phys. Lett.* **2003**, *82*, 657.

(3) Darhuber, A. A.; Valentino, J. P.; Troian, S. M.; Wagner, S. *J. Microelectromech. Syst.* **2003**, *12*, 873.

(4) Chen, J. Z.; Troian, S. M.; Darhuber, A. A.; Wagner, S. *J. Appl. Phys.* **2005**, *97*, 014906.

(5) Bouasse, H. *Capillarité et phénomenès superficiels*; Delagrave: Paris, 1924.

(6) Yarin, A. L.; Liu, W.; Reneker, D. H. *J. Appl. Phys.* **2002**, *91* (No. 7), 4751.

(7) Brzoska, J. B.; Brochard-Wyart, F.; Rondelez, F. *Langmuir* **1993**, *9*, 2220.

10.1021/la7036839 CCC: $40.75
Published on Web 04/10/2008

gradient. Brzoska et al. observed that drops below a critical size, roughly proportional to the inverse of the applied temperature gradient and independent of the viscosity, did not move and attributed this phenomenon to contact angle hysteresis. The drop velocities appeared to fall on a straight line when plotted against the equilibrium radius, and scaled inversely with the viscosity of the liquid, confirming the two main scaling results from a two-dimensional theoretical model presented by the authors, which assumed the drop to be a ridge, infinitely long in one direction. The model is based on an earlier lubrication analysis presented by Brochard,[8] extended in ref 7 to accommodate the consequence of contact angle hysteresis in the form of a resisting force. Brzoska et al. seeded a drop with floating tracer particles to track the surface motion of the fluid. They also presented a photograph of the footprint of a moving drop, showing that it elongated significantly in the direction of motion, with a segment in the middle possessing sides parallel to the applied temperature gradient, similar in shape to large drops moving down an inclined surface under the action of gravity; however, no detailed measurements were reported on the distortion of the footprint of the drop from a circle.

The work of Chen et al.[4] is a systematic follow-up study that builds on work from earlier articles by Darhuber et al.[2,3] in which evidence is offered for the motion of drops of different liquids on a solid surface due to a temperature gradient. Chen et al.[4] constructed an apparatus specifically for the detailed study of the movement of drops on a silanized silicon surface on which a temperature gradient ranging from 2.19 to 3.60 K/mm was imposed. The principal fluid on which a substantial amount of data were obtained and compared with predictions from a two-dimensional model for the motion of a ridge, originating from the work of Ford and Nadim,[9] was squalane. The drops ranged from 1.7 to 3.0 mm in footprint radius. Chen et al. also found that drops below a critical footprint radius did not move in a given temperature gradient, and that this radius was approximately in inverse proportion to the magnitude of the applied temperature gradient. The authors fitted their experimental results to the predictions by adjusting two parameters; one was contact angle hysteresis, and the other was the "slip length". The latter is a parameter with dimensions of length that appears in a modified boundary condition used at the solid surface to accommodate slip. Chen et al. found that the predictions were more sensitive to contact angle hysteresis than to the magnitude of the slip length. Chen et al. also presented data on the velocity of drops of a variety of organic liquids, demonstrating that contact angle hysteresis appeared to play a larger role as the linear alkane chain length of the organic molecule increased. The squalane molecule, even though relatively large, is branched; it does not follow the trend of the linear alkanes in the figure. Chen et al. also noted that drops of 1-propanol, 1-butanol, and 1-hexanol, presumably of comparable size to those of squalane used in their study, did not move in the temperature gradients used. They attributed this to evaporation as well as to the enhanced role of contact angle hysteresis that occurs in the case of these fluids on the surfaces used.

While discussing prior experimental research, we should also mention the work of Sato et al.,[10] who observed silicone oil drops moving on silanized glass surfaces in a reduced gravity environment when subjected to the simultaneous influence of a wettability gradient and a temperature gradient. In some experiments, the authors used a chemically homogeneous surface without a wettability gradient, and reported observing the motion of the drops toward cooler regions on the surface at velocities that increased with increasing droplet volume and decreased when the viscosity of the liquid was increased. Using wettability gradient surfaces, Sato et al. also demonstrated that applying a thermal gradient that enhanced the action of the wettability gradient resulted in more rapid movement of the drops than when only the wettability gradient was used.

We now briefly discuss the literature on theoretical developments on this problem. The principal articles in which models of thermocapillary motion of drops on a solid surface were developed are those of Brochard,[8] Ford and Nadim,[9] and Smith.[11] All three articles employ a two-dimensional analysis in which a ridge formed by translating its cross-sectional shape in the third direction to infinite extent is considered, so that no flow occurs in that third direction. Also, the field variables are independent of position in that direction. Brochard[8] considers a variety of problems involving drops on solid surfaces, including drops whose shapes are influenced by gravity. Lubrication theory is employed to simplify the fluid mechanical analysis, and Brochard also assumes the contact angle to be small so that truncated Taylor series expansions in the contact angle can be used where needed. In addition, when calculating the hydrodynamic force exerted on the drop, the shape of the drop is assumed to be that of a wedge. The model developed by Ford and Nadim[9] is similar to that of Brochard in some respects and different in others. Ford and Nadim consider the motion of a ridge of a specified, but arbitrary, shape. They permit the contact angles to be different at the two ends of the cross section of the drop and use a different way of accommodating slip at the solid surface. It should be mentioned that a traditional description of flow in a drop on a solid surface that assumes the no-slip boundary condition to hold at the solid surface fails because of the occurrence of infinite stresses at the contact line. Therefore, it is common to assume that a small region exists near the contact line where the no-slip boundary condition needs to be relaxed,[8,12,13] or to use a boundary condition everywhere at the solid surface that admits the possibility of slip through a "slip length" parameter. The approach used by Brochard is to carry out the integration of the stress on the solid surface to a point close to the contact line but not all the way to the contact line. Ford and Nadim use a modified slip boundary condition that contains the slip length parameter.

Smith[11] was concerned with issues that are somewhat different from those considered in refs 8 and 9. Smith used a boundary condition at the contact line that relates the speed of the contact line to the contact angle through a specified set of parameters, so that it is not possible to use his approach to infer the velocity of a drop subjected to a temperature gradient on a solid surface. On the other hand, Smith's analysis is comprehensive in that he develops the evolution equation for the shape of the drop, subject to the assumptions of lubrication theory. He then goes on to show that two possible steady states exist: one in which the drop is motionless and the other providing for motion at a constant speed toward colder regions, with a steady shape.

In the present work, we report results from a study of the motion of decane drops on a different type of surface from that used by previous workers, which is relatively easy to prepare in reproducible form. We used poly(dimethylsiloxane) (PDMS)-coated glass slides for the solid surface. Also, in a departure

(8) Brochard, F. *Langmuir* **1989**, *5*, 432.
(9) Ford, M. L.; Nadim, A. *Phys. Fluids* **1994**, *6* (No. 9), 3183.
(10) Sato, M.; Araki, K.; Matsuura, M.; Hasegawa, K.; Endo, A. Proceedings of the 2nd Pan Pacific Basin Workshop on Microgravity Sciences, Pasadena, CA, 2001; Paper IF-1123.
(11) Smith, M. K. *J. Fluid Mech.* **1995**, *294*, 209.
(12) de Gennes, P. G. *Rev. Mod. Phys.* **1985**, *57*, 827.
(13) Cox, R. *J. Fluid Mech.* **1986**, *168*, 169.

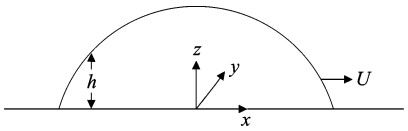

Figure 1. Side view of a drop on a solid surface.

from prior theoretical work, which is limited to two-dimensional ridges, we develop a theoretical analysis based on the lubrication approximation that takes into account the three-dimensional axisymmetric spherical-cap shape of small drops. The theoretical model is an extension of that presented in ref 14 for the motion of a spherical-cap drop on an isothermal surface with a wettability gradient. In the experiments, we used sufficiently small drops, so that their equilibrium shapes are indeed close to that of a spherical cap, with a negligible influence arising from hydrostatic variation of pressure. Results for the measured velocities of the drops are compared with predictions from the theoretical model. We also report some observations on the shapes of the footprints of the drops, which are noncircular.

Next, we present a brief description of the model, followed by sections on the experimental apparatus and procedure, and results and discussion, and we conclude with a few remarks.

2. Analysis

In this section, an approximate theoretical description is developed of the thermocapillary motion of a drop on a solid surface on which a linear temperature field $T_{solid}(x)$ is imposed. A sketch of the system is provided in Figure 1.

Let the height of the drop be $h(x,y)$ and the radius of its footprint, approximated by a circle, be R. Even though the contact angle will, in principle, vary with temperature, the rate of change is relatively small, and we assume here that the contact angle is uniform around the periphery, with a local value θ. The theoretical analysis is based on the lubrication assumption, namely that the maximum height of the drop h_0 is asymptotically small compared with its footprint radius R. The flow in the drop is assumed Newtonian and incompressible, with constant viscosity μ and constant density ρ of the liquid. Quasisteady conditions are assumed. This implies that the times taken for the temperature and vorticity distributions to achieve steady representations within the drop at a given location on the solid surface are small compared with the time required for the drop to move an appreciable distance from that location. The objective of the analysis is to predict the velocity of the drop U. In view of the quasisteady assumption, the net force on the drop at any given location must be zero, and this condition is used to establish a result for the velocity U.

We require that the motion be sufficiently slow that flow-induced deformation of the shape of the drop can be neglected in calculating a leading order result for its speed, an assumption that requires the capillary number $Ca = \mu U/\gamma_0$, where γ_0 is a characteristic surface tension of the liquid−air interface, to be asymptotically small. We also neglect the role of hydrostatic pressure variations in distorting the shape of the drop, assuming the Bond number $Bo = \rho g R h_0/\gamma_0$, where g is the magnitude of the acceleration due to gravity, to be small compared with unity.

It is convenient to solve the problem in a reference frame traveling with the drop, so that the drop appears stationary and the solid surface moves in the negative x-direction with a constant speed U. The lubrication approximation leads to the conclusion that, at leading order, the only nonvanishing velocity component is v_x, and the governing equation for this component is obtained as

$$\mu \frac{\partial^2 v_x}{\partial z^2} = \frac{\partial p}{\partial x} \tag{1}$$

where the leading order contribution to the dynamic pressure field $p(x,y)$ is independent of z. The boundary conditions are

$$v_x(x,y,0) = -U \tag{2}$$

$$\mu \frac{\partial v_x}{\partial z}(x,y,h) = \gamma_T \frac{\partial T_s}{\partial x} \tag{3}$$

where T_s is the temperature at the free surface of the drop and γ_T is the rate of change of the gas−liquid interfacial tension with temperature, which is assumed to be a constant, and is usually negative.

The Peclet number for heat transfer $Pe = h_0 U/\alpha$, where α is the thermal diffusivity of the liquid, is assumed to be sufficiently small that conduction is the dominant heat transfer mechanism within the drop. Coupled with the assumption that the heat transfer to the surrounding air is negligible, this permits one to infer the temperature distribution on the surface of the drop from that imposed on the solid surface. The temperature field in the drop, which obeys the Laplace equation, will be independent of z, so that the distribution of temperature on the free surface will be the same as that existing on the surface of the solid, $T_{solid}(x)$. It already was assumed that T_{solid} is a linear function of x, so that

$$\frac{\partial T_s}{\partial x} = \frac{dT_{solid}}{dx} = G = \text{constant} \tag{4}$$

The solution for the velocity field is

$$v_x = -U + \frac{h^2}{2\mu}\frac{\partial p}{\partial x}\left(\frac{z^2}{h^2} - 2\frac{z}{h}\right) + \left(\frac{h\gamma_T G}{\mu}\right)\frac{z}{h} \tag{5}$$

Because there can be no net volumetric flow across a section at a constant x, we can write

$$\int_0^h v_x(x,y,z)\, dz = 0 \tag{6}$$

Applying this condition to the velocity distribution yields the pressure gradient.

$$\frac{\partial p}{\partial x} = \frac{3\gamma_T G}{2h} - \frac{3\mu U}{h^2} \tag{7}$$

Therefore, the solution for v_x can be rewritten as follows.

$$v = U\left(-1 + 3\frac{z}{h} - \frac{3}{2}\frac{z^2}{h^2}\right) + \frac{h\gamma_T G}{\mu}\left(\frac{3}{4}\frac{z^2}{h^2} - \frac{1}{2}\frac{z}{h}\right) \tag{8}$$

The shear stress exerted by the solid surface on the fluid is given by

$$\tau_w = -\mu \frac{\partial v_x}{\partial z}(x,y,0) = -\frac{3\mu U}{h} + \frac{\gamma_T G}{2} \tag{9}$$

We note that the first term in the right side is an axisymmetric function, because h is axially symmetric, and the second term is a constant.

Integrating the shear stress over the base of the drop yields the hydrodynamic force exerted by the solid on the drop. Taking

(14) Subramanian, R. S.; Moumen, M.; McLaughlin, J. B. *Langmuir* **2005**, *21*, 11844.

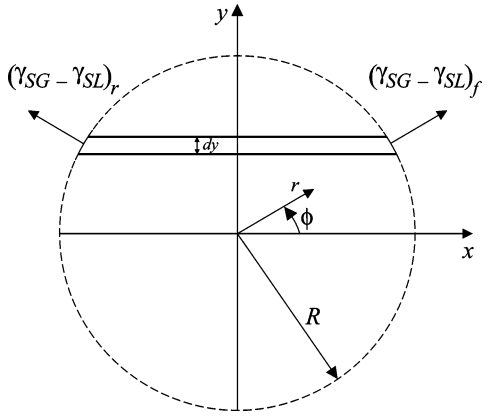

Figure 2. Plan view of the footprint of a drop on a solid surface.

advantage of the axisymmetry of h, the integration is carried out in cylindrical polar coordinates (r,ϕ) on the solid surface.

$$F_h = \int_A \tau_w \, dA = \int_0^{2\pi}\int_0^R \tau_w r \, dr \, d\phi = -6\pi\mu U \int_0^R \frac{r \, dr}{h(r)} + \pi\gamma_T G \int_0^R r \, dr = 6\pi\mu U R[g(\theta,0) - g(\theta,1-\epsilon)] + \frac{\pi R^2 \gamma_T G}{2} \quad (10)$$

where

$$g(\theta,\zeta) = \cot\theta[1 - \ln(\sqrt{\operatorname{cosec}^2\theta - \zeta^2} - \cot\theta)] - \sqrt{\operatorname{cosec}^2\theta - \zeta^2} \quad (11)$$

A result given in ref 14 has been used in obtaining the above expression for the hydrodynamic force. Furthermore, because $h = 0$ at the contact line, the shear stress becomes singular there; therefore, the integration of $r/h(r)$ is terminated a short distance before the contact line is reached; in other words, it is carried out from $r = 0$ to $(1 - \epsilon)R$. This is the reason for the appearance of the small parameter $\epsilon = L_s/R$ in eq 10 where L_s is the extent of the region near the contact line where slip must be accommodated. The distance L_s is assumed to be of the order of molecular dimensions, an estimate based on molecular dynamics simulations reported in ref 15. This subject is discussed further in ref 14.

Force at the Contact Line. Next, we estimate the force exerted by the solid on the drop at the contact line. For this, we use the plan view of the footprint of the drop, assumed to be a circle as noted earlier. A sketch is given in Figure 2.

From Figure 2, it can be seen that the net contact line force that acts on the drop in the x-direction can be written as

$$F_{cl} = 2\int_0^{\frac{\pi R}{2}} \{(\gamma_{SG} - \gamma_{SL})_f - (\gamma_{SG} - \gamma_{SL})_r\} \cos\phi \, dl \quad (12)$$

Here, dl is the differential arc length of the footprint corresponding to the differential change in the polar angle $d\phi$, and it can be written as $dl = R \, d\phi$. The symbols γ_{SG} and γ_{SL} correspond to the solid−gas and solid−liquid interfacial tensions, respectively, and the subscripts "f" and "r" represent "front" and "rear," respectively. The y-component of the force on the drop at the contact line is zero by symmetry.

The solid−gas and solid−liquid interfacial tensions cannot be measured directly; however, they can be related to the equilibrium contact angle and the liquid−gas interfacial tension γ through Young's equation.

$$\gamma_{SG} - \gamma_{SL} = \gamma \cos\theta_e \quad (13)$$

Here, θ_e is an equilibrium contact angle that is an idealization. The solid surface is not at equilibrium, because its temperature varies with position. Therefore, we envision a homogeneous surface at some specified uniform temperature at which the gas−liquid surface tension is γ and define the equilibrium angle on that surface to be θ_e. In a similar manner, in eq 13, the solid−gas and solid−liquid interfacial tensions at that temperature are γ_{SG} and γ_{SL}, respectively.

Making the substitution for $(\gamma_{SG} - \gamma_{SL})$ from eq 13 into eq 12 and using $dl = R \, d\phi$, we obtain the following result.

$$F_{cl} = 2R\int_0^{\frac{\pi}{2}} \{(\gamma \cos\theta_e)_f - (\gamma \cos\theta_e)_r\} \cos\phi \, d\phi \quad (14)$$

To proceed further, we need to know how γ and $\cos\theta_e$ vary around the periphery of the drop. As noted earlier, the variation of the equilibrium contact angle with temperature is usually weak. For decane on PDMS-coated glass surfaces, we measured the rate of change of the equilibrium contact angle, in the range of temperatures we used, to be approximately 0.10°/K, and we neglect this variation as a first approximation. Therefore, we only need to be concerned with the variation of γ with position along the footprint of the drop. The surface temperature of the solid is a linear function of distance. The gas−liquid surface tension has been assumed to be linear in temperature. Therefore, we can write

$$\gamma = \gamma_0 + \gamma_T G x \quad (15)$$

Here, γ_0 is the gas−liquid surface tension at the temperature corresponding to the center of the footprint of the drop; this is the reference surface tension used earlier in defining the capillary and Bond numbers. Using eq 15 to substitute for the values of the surface tension at the front and at the rear in eq 14, the following expression can be obtained for the force exerted by the solid on the drop at the contact line.

$$F_{cl} = 4R^2\gamma_T G \cos\theta_e \int_0^{\pi/2} \cos^2\phi \, d\phi = \pi R^2 \gamma_T G \cos\theta_e \quad (16)$$

By setting the net force exerted by the solid on the fluid, $F_h + F_{cl} = 0$, a result can be obtained for the quasisteady speed of the drop.

$$U = \frac{RG\gamma_T(1 + 2\cos\theta_e)}{12\mu[g(\theta,1-\epsilon) - g(\theta,0)]} \quad (17)$$

For comparison with experimental results, eq 17 is rearranged by combining some of the original variables into a single new variable Ψ.

$$\Psi = \frac{12\mu U[g(\theta_e,1-\epsilon) - g(\theta_e,0)]}{G\gamma_T(1 + 2\cos\theta_e)} = R \quad (18)$$

In doing this, we have interpreted the contact angle θ around the periphery of the drop, assumed constant in the theoretical development, to be the equilibrium value corresponding to the temperature at the center of the footprint of the drop. Likewise,

(15) Thompson, P. A.; Brinckerhoff, W. B.; Robbins, M. O. *J. Adhes. Sci. Technol.* **1993**, *7* (No. 6), 535.

Table 1. Temperature Gradients Used in the Runs and the Range of Values of the Relevant Dimensionless Groups

temperature gradient (K/mm)	Reynolds number	Peclet number	Bond number
1.05	$8.12 \times 10^{-4}-5.51 \times 10^{-3}$	$1.21 \times 10^{-2}-9.50 \times 10^{-2}$	$4.95 \times 10^{-3}-3.24 \times 10^{-2}$
1.85	$2.20 \times 10^{-3}-2.21 \times 10^{-2}$	$2.90 \times 10^{-2}-2.87 \times 10^{-1}$	$4.17 \times 10^{-3}-3.47 \times 10^{-2}$
2.77	$8.71 \times 10^{-3}-7.66 \times 10^{-2}$	$1.01 \times 10^{-1}-8.77 \times 10^{-1}$	$8.22 \times 10^{-3}-4.73 \times 10^{-2}$

the physical properties such as the viscosity and surface tension also are evaluated at the same temperature.

3. Experimental Apparatus and Procedure

The experimental apparatus consists of a steel block with chambers on either side through which liquid from constant temperature baths was circulated to induce and maintain a desired temperature gradient on the surface of the block. A standard glass microscope slide, 24 mm × 50 mm (from VWR), was placed on the block, and thermal cement was used to obtain good thermal contact; on top of this glass slide, a second glass slide, on which a PDMS (poly(dimethylsiloxane)) layer had been deposited using a procedure that will be described later, was placed. The entire apparatus was assembled on a vibration-dampened optical table, and the region of the optical table under use was covered with a cubicle made of plexiglas to minimize the possibility of dust settling on the experimental surface during the runs. Using microthermocouples, the temperature on the top glass surface was measured as a function of distance for the various gradients used in the experiments, and the temperature gradient on the surface was obtained by fitting a straight line to the measured temperatures using the method of least-squares. Care was taken to align the experimental surface to ensure that it was horizontal.

We initially tried thoroughly cleaned glass slides for the experiments and experienced problems with contact angle hysteresis as well as reproducibility. Therefore, we decided to use PDMS coatings on these glass surfaces to obtain reproducibly homogeneous surfaces. The PDMS-coated glass slides for the experiments were prepared using a technique similar to that described in ref 16. Aminopropyl-terminated PDMS of molecular weight 30000 g/mol with two NH_2 end groups was purchased from Gelest, Inc. (DMS-A32). The radius of gyration R_g of the PDMS molecule of this molecular weight is 3.8 nm.[17] Methyl ethyl ketone (MEK) manufactured by Mallinckrodt Baker (JT9319-5, 99.9%) was obtained from VWR. Polyglycidyl methacrylate (PGMA) was synthesized by radical polymerization using the technique described in ref 18 and dissolved in MEK to obtain a 0.03% solution, which was filtered through a 0.2 μm Teflon filter to remove any suspended contaminants.

The glass slides were thoroughly cleaned first with 18.3 MΩ deionized water, followed by rinsing and sonication with acetone and methanol to remove any organic impurities. The slides were then immersed in a base piranha solution (33:67, NH_4OH/H_2O_2) for 30 min to oxidize any residual impurity left on the surface. The slides were rehydrated with deionized water for 10 min and dried by nitrogen and then stored in centrifuge tubes for at least 1 h to ensure that they were completely dry. They were then spin coated at 3000 rpm with the 0.03% solution of PGMA to create an anchoring layer of PGMA. If the relative humidity was greater than 20%, the spin coating was performed within a controlled humidity chamber.

Next, the slides were heated in a vacuum oven for 15 min at 110 °C to cure and cross-link to get a PGMA layer of approximately 2.5 ± 0.2 nm thickness. This layer is a cross-linked polymer film−polymer network used to graft end amino group functionalized PDMS. The slides were then rinsed and sonicated with MEK for 30 min to remove any excess PGMA as well as any contaminants that may have settled on the surface during the spin coating process. After drying with nitrogen, the PDMS (poly(dimethylsiloxane)) with NH_2 end functional groups was spread over the slides coated with the PGMA layer, and the slides were heated in a vacuum oven at 75 °C for 1 h. The NH_2 end functional groups of PDMS react with the epoxy groups of the PGMA anchoring layer so that a well-adhered PDMS layer is formed. It is likely that the PDMS chains are attached by one end; the probability of having two end attachments is small. The PDMS layer is in the brush regime is typically 5.5 ± 0.5 nm thick and is not monomolecular. The flexibility of the surface layer is similar to the bulk flexibility. Using the thickness of the PDMS layer and the relevant physical properties of PDMS, the grafting density is estimated to be approximately 0.11 ± 0.01 chains/nm^2. After preparation, the slides were rinsed and sonicated with MEK to remove any excess PDMS present. Finally, they were dried with nitrogen and stored in centrifuge tubes prior to the migration experiments.

Three different temperature gradients were used in the experiments. In each case, after establishing the temperature gradient, each drop of decane of the desired size was delivered on a fresh track near the warm end of the PDMS-coated glass slide using a World Precision Instruments ultra-microinjection pump (UMP2) and a 50 μL syringe with a Teflon-tipped plunger equipped with glass tips drawn from glass capillaries using a micropipet puller; for ease of delivery, the ends of the tips were made hydrophobic by exposing them to dodecyltrichlorosilane for 15 min. All the drops were observed to move toward the cooler end of the surface. Video images of the drops were captured using two CMOS-based progressive scan monochrome digital cameras (Basler A601f, 0.5 in. sensor size with a firewire video output) connected to PCI IEEE 1394 firewire cards in two computers. One camera captured a side view, while the other was used to obtain a view from the top. The framing rate at the lowest temperature gradient was in the range 2−4 Hz, that at the intermediate temperature gradient was 6−8 Hz, and the rate used for the runs at the largest temperature gradient was 12−16 Hz. The top view was used for subsequent data analysis, with verification provided by the side view images where needed. Because the footprints of the drops were not necessarily circular, the footprint radius was obtained by averaging the diameter measured in the direction of migration and in a direction normal to it and then dividing by 2. Also, it was observed, especially at the largest temperature gradient, that drops decreased slightly in size during the run because of evaporation.

Several drops of different sizes were introduced on a single surface. Reproducibility on a given surface was checked by observing the migration of drops of the same size on different nonadjacent tracks. Experiments were performed at each of three temperature gradients on two different fresh surfaces to check reproducibility from one surface to the next. The footprint radius of the decane drops was varied from approximately 0.6−1.6 mm. The temperature gradients used, along with the range of values of the relevant dimensionless groups, are reported in Table 1. The Peclet and Bond numbers were defined earlier, and the Reynolds number is defined as $Re = \rho U h_0/\mu$, where the symbols were defined in the section on theoretical analysis. In calculating the dimensionless groups, the density, viscosity, and surface tension of decane as a function of temperature were obtained from refs 19 and 20 and fitted to suitable functional forms, and the fits were used to evaluate the needed properties at any given temperature. The surface tension data were found to lie on a straight

(16) Motornov, M.; Sheparovych, R.; Tokarev, I.; Roiter, Y.; Minko, S. *Langmuir* **2007**, *23*, 13.

(17) Arrighi, V.; Gagliardi, S.; Dagger, A.; Shenton, M. *ISIS Facility Annual Report*; Rutherford Appleton Laboratory: Edinburgh, U.K., 2000; Report No. 10229 (available online at http://www.isis.rl.ac.uk/isis2000/reports/10929.pdf).

(18) Iyer, K. S.; Zdyrko, B.; Malz, H.; Pionteck, J.; Luzinov, I. *Macromolecules* **2003**, *36*, 6519.

(19) Vargaftik, N. B. *Handbook of physical properties of liquids and gases*; Hemisphere Publishing Corporation: New York, 1983.

(20) Yaws, C. L. *Yaws' Handbook of Thermodynamic and Physical Properties of Chemical Compounds*; Knovel: New York, 2003.

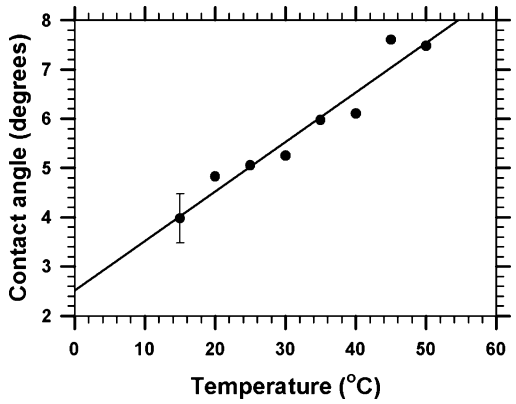

Figure 3. Contact angle of decane plotted against temperature. The symbols represent the data; the best-fit straight line through the data also is shown.

line over the range of temperatures from 0 to 100 °C, and the slope of the best-fit straight line was found to be $\gamma_T = -9.19 \times 10^{-5} \pm 0.01 \times 10^{-5}$ N/(m·K). Details regarding this and the other fits used are given in Appendix F of Pratap's thesis.[21] It is seen from Table 1 that the Bond number is indeed small compared with unity, justifying the assumption made in the analysis regarding this group. The Peclet number is small compared with unity at the low and intermediate gradients, and it approaches unity for the largest drops in the run at the largest gradient. The Reynolds number also is small. Lubrication theory requires only that the product of the Reynolds number and the ratio of the maximum height of the drop to its footprint radius be small compared with unity, an assumption that also is justified.

The stored images from the top view were subsequently analyzed for evaluating the velocity of the drops. Both the front and the rear end of the footprints of the drops were tracked from one frame to the next using Spotlight-8 software.[22] From the location of the center of the footprint of the drop in successive images and the known frame rate, a position versus time curve was obtained. The instantaneous velocity at a given position was estimated as the local slope of a straight line fitted to a set of data points chosen symmetrically about the selected position of the center of the footprint of the drop on the position versus time curve. The number of points was chosen judiciously to minimize the error associated with scatter in the data if too few points are taken, and the error associated with possible curvature in the data if too many points are chosen.

In a separate apparatus, in which the entire PDMS-coated surface was maintained at a fixed temperature that could be adjusted using fluid circulating through a chamber underneath, the contact angle of decane drops was measured as a function of temperature over the range of temperatures employed. Decane drops were placed on the surface, and the temperature was adjusted to the desired value; after sufficient time had elapsed to accommodate the achievement of an equilibrium shape, video images were obtained, and the contact angle was measured using these images. Repeated measurements were averaged to obtain the contact angle at a given temperature. Additional details regarding the experimental apparatus and procedure are given in ref 21.

4. Results and Discussion

The measured contact angles of decane as a function of temperature are displayed in Figure 3, along with a straight line fitted to the data by the method of least-squares. The measurement uncertainty was judged to be approximately ±0.5°, and it is displayed on a typical data point. It is seen that the contact angle of decane increases gently with increasing temperature. The slope of the best-fit straight line is 0.10°/K as noted earlier.

(21) Pratap, V. M. S. Thesis in Chemical Engineering, Clarkson University, 2007.

(22) SpotLight is a software program written by R. Limek and T. Wright, NASA Glenn Research Center, Microgravity Science Division.

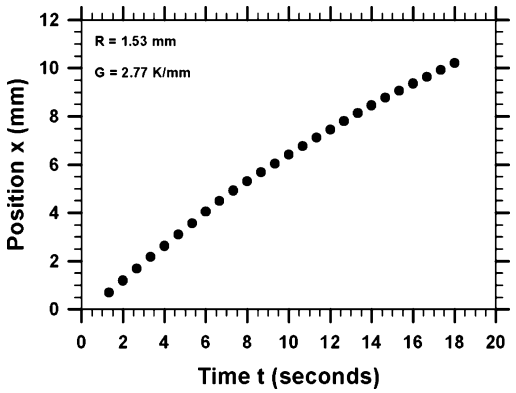

Figure 4. Position of a drop of nominal footprint radius 1.53 mm plotted against time for a gradient $G = 2.77$ K/mm.

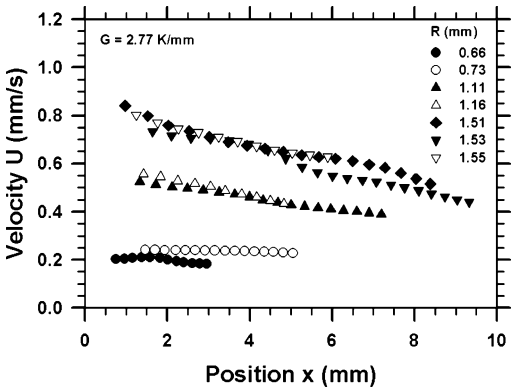

Figure 5. Velocities of drops of different footprint radii plotted against position on the migration surface for $G = 2.77$ K/mm.

Results from a typical migration run at the highest temperature gradient are displayed in Figure 4. The uncertainty in the position measurement is ±0.03 mm and is within the size of the symbols used. To avoid clutter in the drawing, only data from every tenth frame are displayed.

It is seen that the velocity of the drop decreases significantly as it moves toward the cooler end. At the lowest temperature gradient, the position versus time data were found to lie nearly on a straight line over a similar traverse distance. This suggests that the variation of velocity as the drop approaches the cooler end is likely attributable to the variation of physical properties and possibly the change in size of the drop due to evaporation.

A plot of the velocities of several drops inferred from position data at the temperature gradient of 2.77 K/mm is displayed in Figure 5. The uncertainties in velocities, which represent 95% confidence intervals in the slope of a linear fit of position versus time data, are less than or equal to ±0.012 mm/s and are within the size of the symbols used.

Several points are worth noting from Figure 5. First, drops of approximately the same size, introduced on fresh nonadjacent tracks on the surface, are seen to move at approximately the same velocity, providing confidence regarding the reproducibility of the observed behavior. Second, larger drops are seen to move more rapidly than smaller drops. Third, drops of intermediate to large size are seen to decrease appreciably in velocity as they move toward the cold end.

From the measured footprint radii, it was observed that large drops decreased in footprint radius by as much as 5−7% during their traverse. The equilibrium contact angles decrease slightly as the drops move into cooler regions, and therefore, the resulting spreading of the drops should yield correspondingly larger

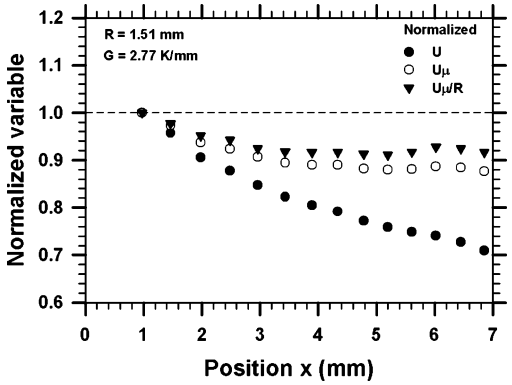

Figure 6. Three different normalized variables plotted against position on the solid surface at $G = 2.77$ K/mm.

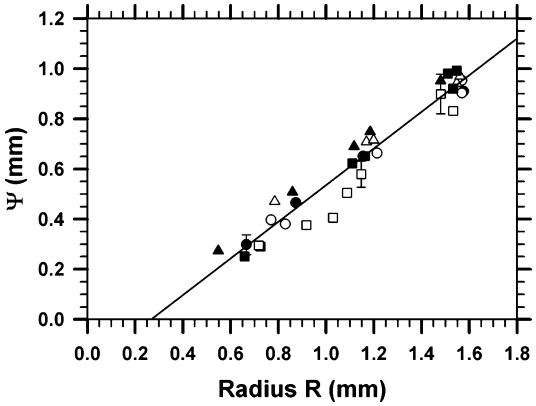

Figure 7. Results from experiments on two different strips and three gradients. The open symbols represent data from strip 1, and the closed symbols represent data from strip 2. The circles correspond to $G = 1.05$ K/mm, the triangles to $G = 1.85$ K/mm, and the squares to $G = 2.77$ K/mm. A straight line fitted to the data by the method of least-squares also is displayed.

footprint radii. The fact that the footprint radius actually decreases during the traverse suggests that the drops undergo some evaporation.

The decrease in velocity during the traverse of a drop can arise both from the decrease in size and the increase in viscosity that accompanies the movement into cooler regions on the surface. Figure 6 is used to determine the relative importance of these two contributions.

Three normalized variables are plotted in Figure 6 for a single experimental run at a gradient of 2.77 K/mm on a drop of nominal footprint radius 1.51 mm. They are U/U_{start}, $(U\mu)/(U\mu)_{start}$, and $(U\mu/R)/(U\mu/R)_{start}$. The subscript "start" refers to the values of the variables at the starting point for which data are presented, and therefore, all three normalized variables begin at a value of unity. Focusing first on the velocity itself, the figure shows that the velocity of this drop decreased to approximately 0.7 times its starting value at the last point for which a data point is displayed. The viscosity and the instantaneous footprint radius of the drop were evaluated at various locations along the traverse, with the viscosity being estimated at the temperature corresponding to the location of the center of the footprint of the drop. It is seen that the variation of the product of the velocity and viscosity is much smaller than that in the velocity itself. As can be seen from eq 17, the predicted velocity of the drop depends linearly on the footprint radius directly, but it also depends on the radius indirectly through the parameter ϵ that appears in the denominator. Calculations made using eq 17 indicate that the dominant dependence on the radius is the direct proportionality that appears in the numerator. Figure 6 shows that scaling out this dominant portion of the dependence of the velocity on the drop size yields an additional small contribution toward removing the variation in the normalized variable during a drop's traverse. This implies that most of the slowing of the drop along its path can be attributed to the increasing viscosity, with a small contribution arising from the reduction in drop size due to evaporation.

From here on, for each experiment, only a single instantaneous velocity measured at a particular location, where the motion of the drop is found to be free from contact line pinning, is reported. Other results such as the radius and aspect ratio (defined later) also are measured at the same location for that experiment. For each gradient, the instantaneous velocities of different drops were measured at the same location on the gradient surface, so that the temperature at the location of the center of the footprint of the drop is the same for drops of different sizes at that gradient. It was not possible to choose the same temperature for drops at other gradients, but, in each case, we were able to obtain velocity data at the same temperature for all the drops moving in a given gradient. As mentioned earlier, the experiments were repeated on two different strips. Data also were obtained from a third strip, but as reported in ref 21, while the results from that strip were internally self-consistent, the drops exhibited far more hysteresis effects. One might conclude that even though the procedure for preparing that surface was nominally the same, the actual surface was sufficiently different from that on the other two strips to lead to substantial hysteresis.

When we plotted data from all the experiments in the form of velocity against drop footprint radius, we found that data from all three temperature gradients yielded approximately the same nonzero intercept on the abscissa. This implied that the velocity of a drop approaches zero at a nonzero critical footprint radius R_c, independent of the value of the temperature gradient. Qualitatively similar behavior, attributed to the effects of contact angle hysteresis, had been noted by Brzoska et al.[7] and Chen et al.; [4] however, the results in both cases show a clear trend of decrease in the critical radius as the temperature gradient is increased. In both refs 4 and 7, silanized silicon surfaces were used, whereas our surfaces are different and are made of PDMS-coated glass. In ref 7, the temperature gradients used were relatively gentle, but the gradients used in ref 4 were of comparable magnitude to those used here. It is possible that our gradients were sufficiently large for the surfaces used in our work to have reached a limiting situation with respect to the effect of contact angle hysteresis. By this, we mean that no matter how large a gradient is applied, a drop of a sufficiently small size may not move because of hysteresis.

In Figure 7, the data from two strips and three different gradients are combined and plotted in the form of Ψ against R for comparison with the prediction from eq 18.

In calculating $\epsilon (= L_s/R)$, we assumed $L_s = 0.5$ nm. The molecular dynamics simulations in ref 15 suggest that the region in which slip needs to be accommodated appears to be of the order of one to two molecular diameters, which is our rationale for selecting this value of L_s. Later, we comment on other values of L_s that were tried.

Eq 18 predicts that the data, when plotted in the form of Ψ against R, should fall on a straight line of unit slope, passing through the origin. It is evident that the data from all three gradients and from both surfaces do indeed cluster around a straight line, subject to some scatter, but the straight line, when extended, does not pass through the origin. The best-fit straight line shown in the figure has a slope of 0.73 ± 0.06 and, when extended, intersects the x-axis at a critical radius $R_c \approx 0.27 \pm 0.08$ mm. For comparison, examination of Figures 2 and 3 in Brzoska et

al.[7] shows $R_c \geq 2$ mm for PDMS drops, and from a plot given in Chen et al.[4] it appears that $R_c \geq 1.6$ mm for squalane drops, both on silanized silicon surfaces. It is evident that the R_c value inferred from the present work on decane drops on PDMS-coated glass slides is much smaller than those values, implying a minimal influence of contact angle hysteresis in the present experiments. Also, as noted earlier, the critical radius is found to be independent of the applied temperature gradient. We interpret this to indicate that perhaps a size limit has been reached on this type of surface for decane drops (in terms of hysteresis); in other words, drops below a certain size will not move, regardless of how large a temperature gradient is used. The empirical approach to modeling contact angle hysteresis used in both refs 4 and 7 involves the idea of using the advancing and receding contact angles on the front and rear, respectively, of the drop in evaluating the force at the contact line. This approach implies that a certain minimal force needs to be exerted on the drop to overcome hysteresis. As a consequence, the critical radius is predicted by these empirical models to be inversely proportional to the applied temperature gradient. A similar extension of the present model was developed in ref 21, yielding the same prediction. However, it is evident that such a modeling approach does not correctly explain the influence of hysteresis in the present experiments. The difficulty arises from the use of advancing and receding contact angles in the evaluation of the contact line force. It is doubtful whether the use of such angles in a model is indeed justified, because the force at the contact line is the difference between the forces exerted by the solid−liquid and solid−gas interfaces on an element of the contact line, suitably decomposed in the direction of motion and integrated around the periphery of the drop. The concept of force equilibrium at the contact line is implicitly invoked in refs 4 and 7 to convert this net force to the product of the gas−liquid surface tension and the cosine of the advancing or receding contact angle. However, it has been argued in ref 23, for example, that at a moving contact line the forces at the contact line are not in equilibrium, and it is the "unbalanced Young force" that causes the advancement of the contact line in the problem of drop spreading. The only empirical way in which we can accommodate our observation of a residual critical radius that is independent of the applied temperature gradient is to write the right side of eq 18 as $R - R_c$ and infer the value of R_c from the fit in Figure 7.

Given the various approximations made in developing the model, it is not surprising that the slope of the best-fit straight line does not match the theoretical value of unity but is somewhat smaller. We found the results to be sensitive to the value of the contact angle. If all the contact angles are reduced by 1° and the data are fitted to a straight line, the slope increases to 0.89, a value that is much closer to the theoretical value of unity. Likewise, if all the contact angles are increased by 1°, then the slope of the best-fit line becomes 0.62. Therefore, a more accurate method for measuring the very small contact angles made by decane on the PDMS-coated surfaces used in the present work might possibly help reduce the discrepancy between the predicted and observed velocities. Also, the footprints of the drops were observed to be deformed from a circle, and deformation of shape is neglected in the approximate theoretical treatment, which can account for some of the differences between predicted and observed velocities. It is satisfying to see the linear scaling of Ψ with R supported by the data on all three gradients, and the linear scaling of the velocity with the temperature gradient implied in eq 18 supported by the data. The other noteworthy aspect mentioned already is that R_c appears to be independent of the temperature gradient G.

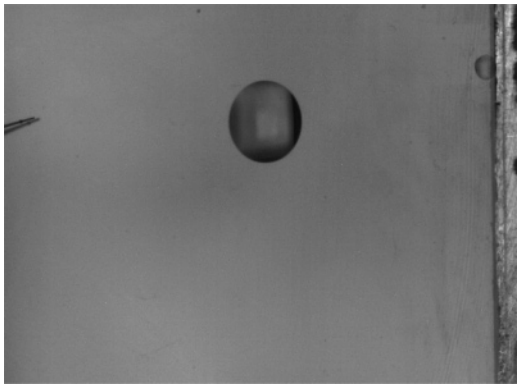

Figure 8. Top view of a decane drop of nominal footprint radius 1.45 mm moving in a gradient of 2.77 K/mm. The aspect ratio of this drop, defined as the ratio of the diameter in the direction of motion to that in the direction perpendicular to it, is 0.88.

We also tried other values of the length of the region L_s in which slip is permitted. The two alternative values tried were $L_s = 2.5$ and 0.2 nm. In both cases, the data still collapsed onto a straight line when plotted in the form of Figure 7, and the statistical measures of the fit were not distinguishable from those for the fit in Figure 7; however, the slope of the best-fit straight line was altered. The slope in the case of $L_s = 2.5$ nm was found to be 0.65, which is considerably smaller than the slope for $L_s = 0.5$ nm used in Figure 7, and farther from the predicted value of unity; when L_s was set equal to the smallest reasonable value of 0.2 nm, the slope was increased slightly to 0.78.

We invoked the quasisteady approximation in developing the theoretical description. The maximum height of the largest drop in the experiments was approximately 0.3 mm. The time required for conduction over this distance is of the order of 1 second, while the viscous relaxation time is approximately 70 ms. During the larger of these two time scales, the drop moved a distance of 0.8 mm, a sufficiently small distance on the surface for the quasisteady state assumption to be a good approximation.

Deformation of the Footprints of the Drops. Brzoska et al.[7] used relatively large drops. When at rest, these drops had a footprint radius up to 10 mm. The footprints of the moving drops were distorted and displayed a shape comparable to those of drops sliding down an incline. Straight line segments were found to separate the advancing and receding portions of the contact line of the drop. The squalane drops studied by Chen et al.[4] were found to be slightly distorted. The authors report that the drops were elongated in the direction of motion, with the diameter in the direction of motion being no more than 1.04 times the diameter in a perpendicular direction on the solid surface. Moumen et al.,[24] who performed experiments on the motion of tetraethylene glycol drops on silanized silicon surfaces with a wettability gradient, observed no measurable deformation of the footprint from a circular shape. The equilibrium contact angle of a typical drop varied significantly around the periphery, and yet the footprints remained sensibly circular. In the present case, we found the drops to be elongated in the direction on the solid surface that is perpendicular to that of motion. A typical top view of a drop moving in a temperature gradient of 2.77 K/mm is shown in Figure 8.

We measured an aspect ratio defined as the ratio of the diameter in the direction of motion to that in a perpendicular direction on

(23) Brochard-Wyart, F.; de Gennes, P. G. *Adv. Colloid Interface Sci.* **1992**, *39*, 1.

(24) Moumen, M.; Subramanian, R. S.; McLaughlin, J. B. *Langmuir* **2006**, *22*, 2682.

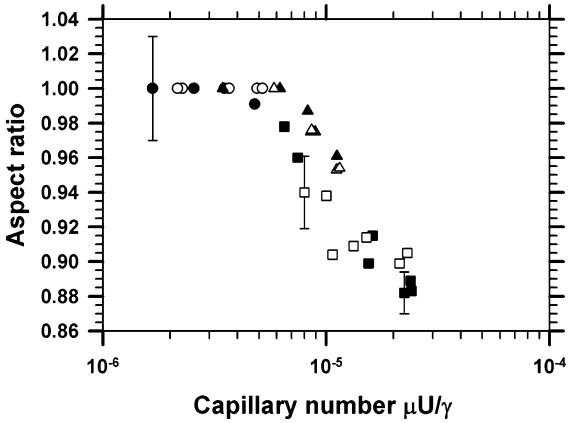

Figure 9. Aspect ratio of the drops plotted against the capillary number for two strips and three different temperature gradients. The open symbols represent data from strip 1, and the closed symbols represent data from strip 2. The circles correspond to $G = 1.05$ K/mm, the triangles to $G = 1.85$ K/mm, and the squares to $G = 2.77$ K/mm.

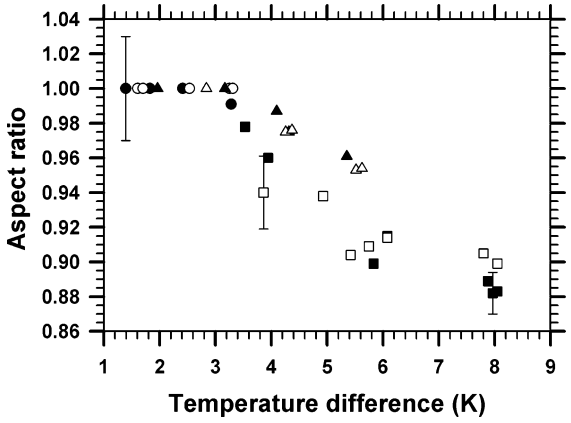

Figure 10. Aspect ratio of the drops plotted against the temperature difference across the footprint of the drop for two strips and three different temperature gradients. The open symbols represent data from strip 1, and the closed symbols represent data from strip 2. The circles correspond to $G = 1.05$ K/mm, the triangles to $G = 1.85$ K/mm, and the squares to $G = 2.77$ K/mm.

the solid surface for each drop. This aspect ratio did not change significantly during the traverse of a given drop, and the values we decided to use are those measured at the same location where the velocity data are reported in Figure 7. The flow-induced shape deformation in low Reynolds number motion depends on the capillary number. Therefore, we have plotted the aspect ratio against the capillary number in Figure 9 to see whether indeed the distortion of the footprint correlates with that dimensionless group. Data from all three gradients and from two surfaces are shown in the figure.

It is seen that, indeed, the aspect ratio appears to be correlated with the capillary number; however, we add a note of caution that the parameter that most influences the capillary number in these experiments is the velocity of the drop, which increases with drop size, and increases as the temperature gradient is increased. Therefore, the capillary number strongly correlates with the temperature difference across the footprint of the drop. To demonstrate this connection, the data in Figure 9 are plotted in Figure 10 in the form of the aspect ratio against the temperature difference across the footprint of the drop.

Because the equilibrium contact angle depends on temperature, the larger this temperature difference, the larger will be the variation of the contact angle around the periphery of the drop, which will also lead to distortion of the footprint of the drop from a circular shape. One can argue that it is the variation in the equilibrium contact angle that causes the footprint to distort and that the capillary number only influences the distortion of the shape of the free surface of the drop; however, the dynamic contact angle is influenced by the motion of the drop, which in turn is affected by its shape deformation. We note that comparable variations of the equilibrium contact angle around the periphery of the drops in experiments on motion in a wettability gradient[24] did not lead to appreciable deformation of the footprint from a circular shape. Thus, it is evident that the deformation of the footprint shapes in the thermocapillary migration experiments is a complex issue requiring further study to unravel its correct origin.

5. Concluding Remarks

We have presented a lubrication theory-based model for the thermocapillary motion of spherical-cap drops on a solid surface and experimental results on decane drops moving on a PDMS-coated glass slide that appear to confirm the principal scalings of the theoretical model. These include the scaling of the velocity of the drop with the drop size and the applied temperature gradient. The experimentally measured velocities are smaller than the predicted values, likely because of the simplifying assumptions used to develop the theoretical model.

Two additional observations worthy of note are that the footprints of the drops were significantly deformed from a circle; this deformation correlates well with the temperature difference across the footprint of the drop. One can conclude that the distortion is possibly due to the variation of the contact angle around the periphery of the drop, or that it also is influenced by the motion of the drop through the capillary number. It is not possible to decouple these influences using the present observations. The second important observation we made is that the effects of contact angle hysteresis appear to be much weaker in the present work than in previous studies.[4,7] The critical footprint radius, which represents the radius of the drop that is just prevented from moving due to hysteresis, was estimated to be 0.27 mm, a value significantly smaller than those found in refs 4 and 7. We also found the critical footprint radius to be uninfluenced by the applied temperature gradient.

Acknowledgment. This work was supported in part by NASA Grant NAG3-2703. We are grateful to Professor Sergiy Minko and Mr. Roman Sheparovych for their generous help in the preparation of the PDMS-coated glass slides used in the experiments in their laboratory, and in providing detailed information regarding the properties of the PDMS layer and the preparation process reported in this work.

LA7036839